Fatigue and leakage behaviour of corroded cast iron pipes.

JOHN, EDA, BOXALL, JB, COLLINS, RP, BOWMAN, ET and SUSMEL, Luca

Water Research 301 (2026) 126046

Contents lists available at ScienceDirect

Water Research

journal homepage: www.elsevier.com/locate/watres

Fatigue and leakage behaviour of corroded cast iron pipes

E.D.A. John [a,*], J.B. Boxall [a], R.P. Collins [a], E.T. Bowman [a], L. Susmel [b]

[a] School of Mechanical, Aerospace and Civil Engineering, Sir Frederick Mappin Building, The University of Sheffield, Mappin Street, Sheffield S1 4DT, UK
[b] Materials and Engineering Research Institute, Sheffield Hallam University, Harmer Building, Sheffield S1 1WB, UK

HIGHLIGHTS

- New understanding of the effect of pit shape on pipe strength and leakage behaviour.
- Destructive fatigue experiments of cast iron pipes using bending and pressure loads.
- Small cracks can close and stop leaking under high positive pressures.
- Pit-stress alignment significantly affects pipe strength and leak stability.
- Pit shape measurements would improve pipe condition assessment accuracy.

GRAPHICAL ABSTRACT

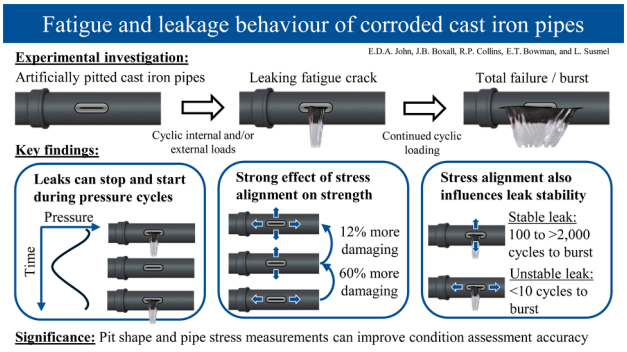

ARTICLE INFO

Keywords:
Water distribution systems
Cast iron
Leakage
Fatigue crack
Corrosion pit
Pipe burst

ABSTRACT

This research explored the hypothesis that different corrosion pit and multiaxial stress alignments cause a significant change in the fatigue strength and leakage behaviour of grey cast iron pipes. Destructive laboratory experiments were used to characterise the fatigue strength and failure mechanisms, including leak-to-burst behaviour. The experiments subjected the pipes to cyclic internal pressure and/or bending loads to cause stresses acting in different directions for a range of artificial pit shapes, including long, narrow pits for the first time. These unique experiments revealed that small cracks in cast iron pipes can close and stop leaking even under high positive water pressures, which has significant implications for leak modelling and detection. Small corrosion pits with stress alignments that caused a high stress concentration were shown to extend the leak-to-burst interval by about two orders of magnitude due to stress concentration effects of the pit. Such pits will progress to catastrophic burst behaviour more slowly than from small initial cracks under uniform wall loss or lower stress concentration pits. From a leakage onset perspective, the fatigue strength reduction caused by long, narrow corrosion pits was found to change by about 60 % depending on the applied stress direction, showing the importance of considering pit-stress alignment in damage assessment and modelling. This research has found that corrosion pit shape, and the relative alignment of the pipe wall stresses, can substantially affect the ability of cast iron pipes to withstand cracking, as well as affecting the stability of leaking cracks once formed. These findings can be utilised to improve cast iron pipe condition assessment and leak detection techniques.

* Corresponding author.
E-mail address: e.d.john@sheffield.ac.uk (E.D.A. John).

https://doi.org/10.1016/j.watres.2026.126046
Received 16 January 2026; Received in revised form 7 April 2026; Accepted 29 April 2026
Available online 30 April 2026

Nomenclature

FEA	Finite element analysis
GCI	Grey cast iron
SWT	Smith-Watson-Topper (multiaxial fatigue criterion)
WDN	Water distribution network
a_{cr}	Critical crack half-length
E	Elastic modulus
F	Bending load
F_{an}	Fatigue average notch effect
$K_{f,ES}$	Fatigue strength reduction factor predicted by the Effective Volume approach, coupled with the Smith-Watson-Topper criterion
K_{IC}	Fracture toughness
K_t	Stress concentration factor, equal to the maximum linear-elastic stress divided by the net ($K_{t,n}$) or gross stress ($K_{t,g}$)
k_0	Negative inverse slope of the reference SN-curve
M_{ES}	Material constant for the Effective Volume approach coupled with the SWT criterion
N_A	High-cycle fatigue reference cycles to failure/leakage
N_b	Number of load cycles to burst
N_f	Number of load cycles to failure/leakage
n	Number of non-runout experiments
P	Pressure load
R	Load ratio, equal to minimum applied cyclic stress divided by maximum applied cyclic stress
T_{RMS}	Mean square error of prediction scatter
$V_{eff,SWT}$	Effective Volume calculated in terms of the SWT criterion. Subscript 0 indicates the Effective Volume of the reference condition
V_i	Volume of element i
$\varepsilon_{n,a}$	Critical plane normal strain amplitude
σ_A	High-cycle fatigue reference stress amplitude
σ_a	Stress amplitude. Subscript (i) indicates the stress amplitude applied during the i th experiment
$\sigma_{a,net}$	Net stress amplitude
$\sigma_{a,SWT}$	Smith-Watson-Topper equivalent uniaxial fully reversed stress amplitude. Subscript i indicates the SWT equivalent stress experienced by the i th element in an FEA model.
$\sigma_{a,SWT,max}$	Maximum value of the SWT criterion at the notch/pit, or the greatest SWT equivalent stress amplitude experienced by any element in an FEA model.
σ_n	Stress applied normal to a crack
$\sigma_{n,max}$	Critical plane maximum normal stress
σ_{net}	Net stress
$\sigma_{Peak,LE}$	Maximum linear-elastic stress
σ_{UTS}	Ultimate tensile strength
σ_x, σ_y	Stress acting in the x and y directions, respectively

1. Introduction

Leakage from water distribution pipes must be reduced to improve the drought resilience of water supplies and reduce water stress (National Infrastructure Commission, 2018; UN-Water, 2021). Leakage from Water Distribution Networks (WDNs) in the UK is typically estimated at close to 20 % of water put into supply (National Infrastructure Commission, 2018; Sanders et al., 2022). In North America average WDN leakage is 10 %, with some states at 20 % (Folkman, 2018), while in Europe France's leakage rate is at 20 %, Italy's is 35 % and Ireland's is 45 % (Sanders et al., 2022). These figures illustrate the global scale of the leakage problem. Sanders et al. (2022) identified that to meet the UK's 2050 target for halving leakage water companies will need to find and fix the small leaks that cause "background" leakage (leaks that are below current detection and location methods) and prevent new leaks through proactive asset management practices.

The leakage estimates provided by water companies in England and Wales as part of the Price Review 2024 submissions, and summarised in Table 1, show that 65 % of total leakage is thought to be due to distribution main losses making these mid-sized pipes a target for leakage reduction measures. Distribution mains pipes in the UK typically have diameters of 3″ to 6″ (75 to 150 mm) and about 41 % of pipes, by length, in this diameter range are Grey Cast Iron (GCI) (UKWIR, 2021). GCI is often identified as requiring a higher rate of repairs per unit length than other pipe materials (Barton et al., 2019; Boxall et al., 2007; Folkman, 2018; Rezaei et al., 2015) making these pipes a key target for leakage reduction measures.

Table 1
Estimated leakage breakdown for the 10 largest water utilities* (by population served) in England and Wales for 2022–2023 from the Price Review 24 data tables.

	Leakage upstream of distribution mains (ML/d)	Distribution main losses (ML/d)	Customer supply pipe losses (ML/d)	Total leakage (ML/d)
Combined leakage for 10 largest utilities	313.1	1765.1	621.5	2699.7
Proportion of total leakage	12 %	65 %	23 %	

* Data sources: Anglian Water (2024); Dwr Cymru (2024); Northumbrian Water (2024); Severn Trent Water (2024); South West Water (2024); Southern Water (2024); Thames Water (2024); United Utilities (2024); Wessex Water (2024); Yorkshire Water (2024).

To proactively replace GCI pipes before they start to leak, asset managers must be able to assess the condition and remaining service life of pipes. To develop effective techniques for detecting small leaks the form and behaviour of these leaks must be known. Both aspects require a good understanding of the mechanisms behind leak formation in GCI pipes.

GCI pipes are vulnerable to a unique form of corrosion pitting, known as graphitic corrosion, where the iron matrix is replaced by a corrosion product that can maintain the original shape of the iron, but is much weaker (Logan et al., 2014; Makar and Rajani, 2000; Seica and Packer, 2004). Seica and Packer (2004) and Yamamoto et al. (1983) both found that the strength of the graphitic corrosion residue is negligible relative to the strength of the remaining iron. As a result, from a structural perspective, corrosion pits are often modelled as air filled notches (Fahimi et al., 2016; Zhang et al., 2017). As notches, corrosion pits cause stress concentrations when service loads are applied to GCI pipes, acting as initiation points for cracks that allow leakage (Atkinson et al., 2002; Makar, 2000; Rathnayaka et al., 2017; Zhang et al., 2017). Previous investigations indicate that corrosion pits penetrating at least 80–90 % through a pipe's wall are required to cause failure under internal pressure service loads (John et al., 2024b; Rathnayaka et al., 2017). The ability to predict when a leaking crack will form at the base of a particular corrosion pit would enable proactive replacement of GCI pipes before they start leaking. Given the amount of existing leakage it is likely that a large number of such small cracks exist. Hence it is also vital to develop understanding of when and which of these small cracks are most likely to develop into catastrophic failures such that these can be identified and prioritised for repair.

The time-variable and cyclic nature of the loads experienced by water pipes (e.g. daily cycles of and transient internal water pressures,

dynamic traffic loads, and soil movement linked to the weather) (Chan et al., 2015; Jara-Arriagada and Stoianov 2022; Robert et al., 2020) means that initial leaking cracks in GCI pipes are likely to form through a fatigue crack growth mechanism (Barton et al., 2019; Brevis et al., 2015; John et al., 2024a). Internal water pressure loads cause hoop stresses, whereas bending loads caused by vertical loads on a poorly supported pipe (Elmrom, 2021; Rajani and Tesfamariam, 2004) or by soil movement (Chan et al., 2015) tend to cause axial stresses which act perpendicular to the hoop stress. Asymmetric notches amplify stresses to a different degree depending on the alignment of the notch and stress direction (Pilkey and Pilkey, 2008), meaning that the interaction between corrosion pit shape and the applied stress direction is likely to be important in determining the remaining life of a GCI pipe. Inspections of exhumed GCI pipes have revealed a wide range of pit shapes including long narrow axially-aligned pits with a high aspect ratio (Jara-Arriagada and Stoianov 2024; Makar, 2000) and large flat-bottomed corrosion patches (Fu et al., 2023; Soltani Asadi and Melchers, 2018). Previous research has shown via experiments the significant effect of pits on the static and fatigue strengths of GCI pipes (John et al., 2026; Zhang et al., 2017), but have not explored the interaction between pit alignment and stress application direction.

To develop effective detection techniques for small leaks it is essential to understand the nature and behaviour of very early-stage leaks. For example, acoustic and hydraulic model-based leak detection techniques both require information about the leak behaviour to be effective (Fox et al., 2018; He et al., 2026; Li et al., 2022; Yu et al., 2023). Rathnayaka et al. (2017) showed using a small number of experiments that, under a ramped internal pressure load, cracks a few mm long in GCI pipes can allow water loss and that a stable leak-before-burst period can exist. Rathnayaka et al. (2018) generated a crack in the same way but cycled the pressure once the crack had formed, showing that existing leaks may grow due to fatigue loading. However, the behaviour of leaking cracks initiated through fatigue loading has not previously been explored, nor has the interaction between pit shape and the nature of the resultant leak.

The research presented in this paper explored the hypothesis that different corrosion pit and multiaxial stress alignments cause a significant change in the fatigue strength and leakage behaviour of GCI pipes. If proven, this hypothesis implies that corrosion pit shape holds important information about the residual strength and likely failure behaviour of a GCI pipe, which could be utilised for pipe condition assessment.

2. Material and methods

It was anticipated that pits with higher aspect ratios (e.g. long, thin pits) are more sensitive to different pit-stress alignments than pits with aspect ratios close to one (e.g. circular pits) or uniform wall loss. This research therefore aimed to compare the fatigue and leakage behaviour of high-aspect ratio pits with low-aspect ratio pits and uniform wall loss. The fatigue behaviour of GCI pipes featuring uniform wall loss and rounded pits has previously been characterised (John et al., 2024c, 2026), however, the leakage behaviour of fatigue cracks formed at these types of corrosion has not. Therefore, this research used destructive laboratory experiments to characterise the leakage behaviour of GCI pipes featuring rounded pits and uniform wall loss with further experiments conducted to explore both the fatigue and leakage behaviour of GCI pipes with high-aspect ratio pits. Long, narrow axially aligned pits have been found in exhumed GCI pipes (Jara-Arriagada and Stoianov 2024; Makar, 2000), whereas long, narrow circumferentially aligned pits do not appear to be reported. Therefore, pipes with axially aligned artificial pits were used to test the sensitivity of high-aspect ratio pits to different stress alignments. Additionally, once characterised and understood, translating the fatigue cracking and leakage behaviour of axially aligned pits to circumferentially aligned pits would be straightforward as the effects of axial and hoop stresses would effectively be swapped.

To perform these destructive fatigue experiments, the recently developed biaxial fatigue pipe testing apparatus (John et al., 2025) shown by Fig. 1a was used to apply cyclic bending (Fig. 1b) and/or cyclic internal pressure (Fig. 1c) loads to GCI pipe specimens. Using the biaxial fatigue testing apparatus it was possible to explore the effect of different pit and stress alignments by applying stress parallel to the pit's long axis with a bending load (Fig. 1d) and applying stress perpendicular to the pit's long axis with an internal pressure load (Fig. 1f). Out-of-phase biaxial loading using both the bending and internal pressure loads (Fig. 1e) was also tested due to it's potential to cause greater damage to GCI pipes (John et al., 2026).

The cycles-to-leakage of each fatigue experiment were observed to quantify the impact of each pit/stress combination on the pipe's fatigue strength. To establish whether the damaging effect of the different pit/stress combinations could be predicted, the cycles-to-leakage results were used to test the effectiveness of the Net Stress and Effective Volume notch fatigue models, which have previously been found effective at predicting the damaging effect of pits in GCI pipes (John et al., 2026). Once a leak had formed, additional stress cycles were recorded using pressure transducers and / or high-speed cameras to capture this rarely seen, under controlled conditions, phenomenon.

2.1. Cast iron pipe specimens

To enable repeatable fatigue experiments with controlled corrosion damage, artificial pits (i.e. machined notches) were added to as-new pipes to make test specimens. This approach was justified by the negligible strength of graphitic corrosion residue relative to iron (Seica and Packer, 2004; Yamamoto et al., 1983). BS 416–2 soil pipes (British Standards, 1990) were used to represent as-new GCI pipes. These soil pipes have very similar graphite microstructures (flake graphite with lengths <80 μm), tensile stress-strain properties (σ_{UTS} = 229 MPa, E = 82 GPa), and uniaxial fatigue strengths to exhumed spun-cast grey iron water pipes, making them a suitable representation of GCI water pipes in destructive experiments (John et al., 2024b, 2024c). BS 416–2 pipes with a nominal diameter of 50 mm were used for testing as they had a wall thickness to external diameter ratio of 0.06 which is the same ratio as for UK 4″ Class C spun-cast grey iron water pipes (British Standards Institution, 1958).

The local stresses in the gauge section of the pipe specimens during the experiments were critical and therefore carefully controlled. The specimen length (630 mm) and bending load point and support spacings (200 mm and 480 mm, respectively) were selected via a preliminary FEA investigation to ensure that uniform stresses and strains were achieved in the central gauge section of pipes and that boundary effects were avoided. Verification testing returned measured strains within ±10 % of the predictions (John et al., 2025), showing that the intended strains were applied and boundary effects were controlled.

Three types of specimens were produced to investigate the effect of uniform wall loss and low-aspect ratio pits on the leakage behaviour and leak-to-burst interval of the pipes. These specimen types represented uniform corrosion (Fig. 2a), and round pits with sharp and blunt bases (Fig. 2b and Fig. 2c). The uniform wall loss and round pits penetrated approximately halfway through the pipes' walls.

To investigate the sensitivity of the pipes' fatigue strength and leakage behaviour to high-aspect ratio pits, pipe specimens with 20 mm long, 5 mm wide, axially aligned pits were manufactured, as shown by Fig. 3. A relatively sharp 0.1 mm pit root radius was chosen, giving the pit a 'V' cross-section, as previous research has shown that sharper pits give similar fatigue strengths as blunt pits, but with more consistent results (John et al., 2026). The internal diameter of the pipes varied from the average value by up to ±1 mm making manufacturing pits with a consistent depth challenging, particularly for deeper pits where small differences in remaining wall thickness causes a disproportionately large change in pipe stresses. A remaining wall thickness of 1.20 mm at the

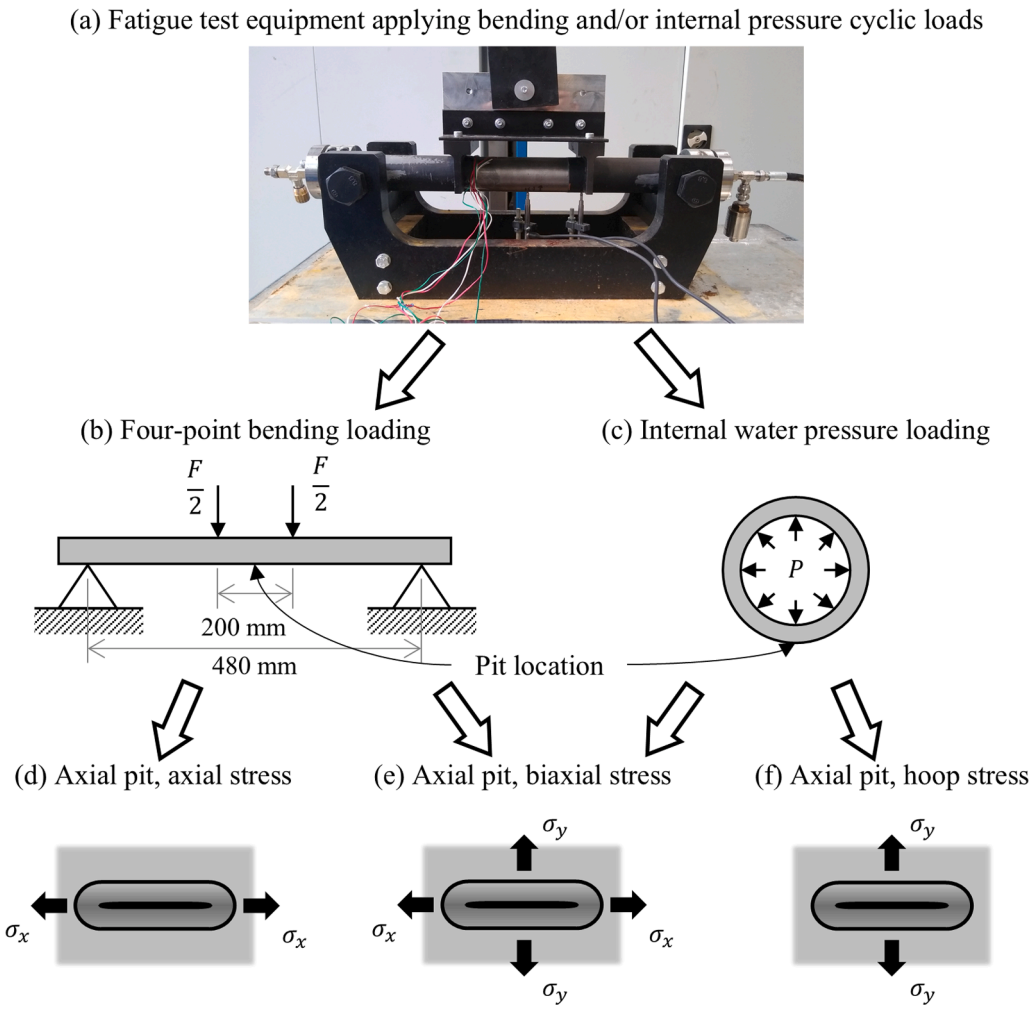

Fig. 1. Illustration of how the fatigue test equipment developed (a) was able to apply four-point bending fatigue loading (b) and internal pressure fatigue loading (c) to pipe specimens, enabling experiments using either axial stresses (d), hoop stresses (f), or combined biaxial stresses (e).

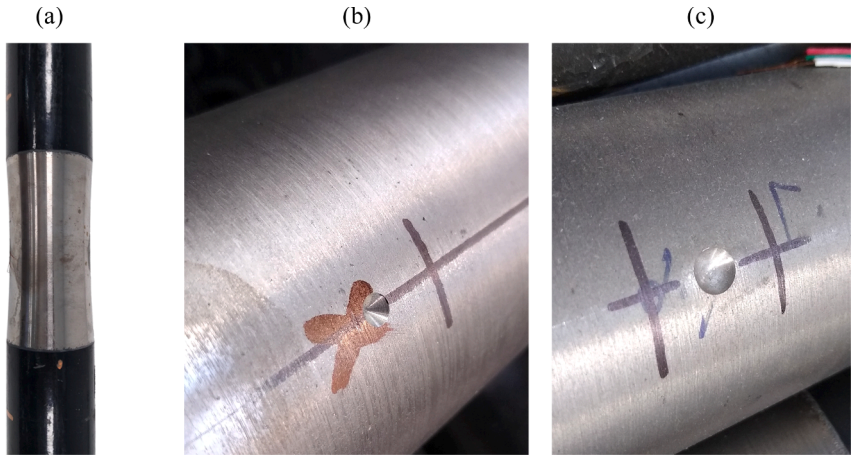

Fig. 2. Images showing the (a) uniform wall-loss (radius 715.0 mm), (b) sharp circular pit (root radius 0.1 mm), and (c) blunt circular pit (root radius 4.0 mm) artificial corrosion geometries tested to investigate leakage behaviour.

base of the pit was used, corresponding to a wall loss of about 70 %, to balance these manufacturing constraints with the expected >80 % wall loss required to cause failure under service loads. In practice, specimens had remaining wall thicknesses between 0.95 mm and 1.49 mm. Accurate post-test measurements of the pits were used in subsequent analyses.

2.2. *Fatigue experiments*

The combinations of artificially corroded pipe specimens and cyclic

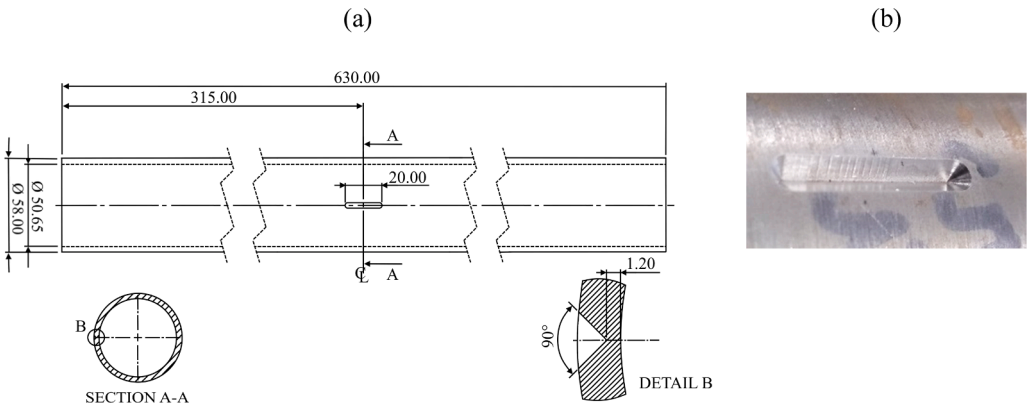

Fig. 3. (a) Dimensioned drawing of the axially notched cast iron pipe specimens tested under bending and internal pressure fatigue loads (dimensions in mm, not to scale) and (b) an image showing a close-up of an axial pit as machined.

loading shown by Table 2 were tested using the equipment shown by Fig. 1a. This equipment was carefully verified to ensure that the intended cyclic stresses were applied to pipe specimens (John et al., 2025). The water pressure containment system converted pipes into closed-ended pressure vessels. This resulted in an additional in-phase axial stress with half the magnitude of the hoop stress caused by the water pressure load. This additional stress was accounted for in subsequent analysis; however, the logarithmic relations that govern fatigue behaviour mean that a stress with a 50 % lower amplitude is considerably less damaging and therefore unlikely to substantially effect results.

Two different 'failure' definitions were applied to experiments, corresponding with the research's aim of investigating both the fatigue strength and leakage behaviour of GCI pipes. The first definition was 'cycles-to-leakage', which was the number of load cycles from an experiment beginning to the formation of a crack that allowed any water loss. This definition was used to explore the fatigue strength of the pipes. The second definition was 'cycles-to-burst', which was the number of load cycles between the onset of leakage and unstable crack propagation that resulted in the structural failure of the pipe (i.e. burst). This definition was used to explore the leak-to-burst behaviour of the pipes. The onset of leakage and burst were detected using a high-speed camera, and pressure and strain measurements. The high-speed camera was available for all the sharp axial pit and uniform wall loss biaxial loading experiments. For other experiments, water at a low pressure was sealed into the pipes, so it was possible to use pressure measurements to detect the onset of leakage here.

Previous research has estimated around 3 to 10 years would be required, once corrosion has grown to a sufficient extent, for fatigue failure of a GCI pipe to occur, which corresponded to approximately 10^4 to 10^7 load cycles (Brevis et al., 2015; Jiang et al., 2019; John et al., 2024b). This falls within the high-cycle fatigue cracking regime of grey cast iron (10^2 to 10^7 load cycles (Weinacht and Socie, 1987)) where elastic strains dominate and a linear relationship exists between cycles to failure and stress amplitude (Socie and Marquis, 1999; Weinacht and Socie, 1987). Therefore, the experiments aimed to cause high-cycle fatigue failures. To avoid excessively long test durations, the loads applied during experiments were selected to cause cycles-to-leakage of at least 10^3 load cycles and no $>10^5$ load cycles. In most metals, at fatigue lives (i.e. cycles-to-leakage) less than about 10^3 cycles plastic strains typically become more important, meaning the fatigue behaviour of a material changes and linear-elastic analysis becomes invalid (Carpinteri et al., 2017; Fatemi and Shamsaei, 2011).

Table 2
Experiment matrix showing the combinations of loading and artificial corrosion tested, and the motivation behind each test set.

Pipe specimen	Motivation of experiment sets completed		
	Bending loading (Fig. 1d)	Internal pressure loading (Fig. 1f)	Out-of-phase biaxial loading (Fig. 1e)
Uniform wall loss (Fig. 2a)	Leakage behaviour		Leakage behaviour
Sharp, circular pit (Fig. 2b)	Leakage behaviour		
Blunt, circular pit (Fig. 2c)	Leakage behaviour		
Sharp, axial pit (Fig. 3)	Fatigue and leakage behaviour	Fatigue and leakage behaviour	Fatigue and leakage behaviour

A minimum of three experiments were completed per configuration shown in Table 2, as this was just sufficient to indicate the expected behaviour and variability of each configuration owing to the practical limitations associated with running these complex tests. Previous work has quantified the scatter in fatigue strength of the cast iron material tested (John et al., 2024c). Some additional internal pressure loading experiments were performed as 'scoping' experiments to determine the loading required to give failures within the 10^3 to 10^5 cycles-to-leakage range.

The target load ratio (minimum load divided by maximum load) for all experiments was 0.1, reflecting the fact that real loading on pipes usually has a mean stress greater than zero. In accordance with the aim of causing high-cycle fatigue failures the internal pressure loads applied had amplitudes between 2.0 and 6.3 MPa, with the variation due to the initial trial-and-improvement process to select the loading and to account for as-manufactured specimen wall thickness variation. These internal pressure loads were considerably greater than real water distribution network pressures owing to the relatively shallow depth of the pits tested discussed above; deeper pits would have allowed realistic experimental pressures, but these could not be manufactured consistently. Bending loads were applied at 4 Hz, internal pressure loads at 2 Hz, and biaxial loading was applied at 1.7 Hz, each of which correspond to the maximum possible loading frequency of the configuration.

2.3. Fatigue data analysis and cycles-to-leakage estimates

To assess the effect of a particular pit/stress combination on the pipes' fatigue behaviour the net stress concentration factor, $K_{t,n}$, and fatigue average notch effect, F_{an}, were calculated and compared. $K_{t,n}$ is the ratio of the maximum linear-elastic stress, $\sigma_{Peak,LE}$, to the net stress, σ_{net}, and indicates the severity of a stress raiser, such as a corrosion pit:

$$K_{t,n} = \frac{\sigma_{Peak,LE}}{\sigma_{net}} \quad (1)$$

The net stress of a pitted pipe is the stress experienced by an identical pipe but with uniform wall loss of the same depth as the pit. The maximum and net stresses for each experiment configuration were

calculated using the Finite Element Analysis detailed below.

F_{an} uses experimental data to quantify how damaging a pit and load combination is relative to the un-pitted or uniform wall loss case by providing an effective fatigue strength reduction factor. The F_{an} calculation assumes that the slope of the fatigue curve is the same for the pitted and un-pitted cases, which is a reasonable assumption for GCI (John et al., 2026):

$$F_{an} = \frac{1}{n}\sum_{i=1}^{n}\left\{\frac{\sigma_{A,o}}{\sigma_{a(i)}\left[\frac{N_{f(i)}}{N_A}\right]^{1/k_0}}\right\} \tag{2}$$

where: n is the number of experiments in the data set; $\sigma_{a(i)}$ is the stress amplitude applied during the i th experiment; $N_{f(i)}$ is the observed cycles-to-leakage of the i th experiment; N_A is the high-cycle reference cycles-to-leakage, equal to 10^6 cycles; and $\sigma_{A,o}$ and k_0 are the high-cycle reference stress amplitude and negative inverse slope of the reference case. Bending loading is known to increase the fatigue strength of GCI pipes by about 43 % due to the non-uniform stress distribution caused (John et al., 2026). To enable F_{an} to capture the effect of pits independently of the bending load effect different reference values of $\sigma_{A,o}$ and k_0 were used depending on the load type applied. For internal pressure experiments, the un-notched uniaxial values of $\sigma_{A,o}$ and k_0 were used, equal to 85.8 MPa and 11.5, respectively (John et al., 2024c). For bending experiments the un-notched bending values of $\sigma_{A,o}$ and k_0 were used instead, equal to 76.8 MPa and 11.2, respectively (John et al., 2026). F_{an} was always calculated in terms of net stresses.

Due to its simplicity of calculation, the net stress is frequently used in practice to account for the effect of corrosion pitting on the stresses experienced by GCI pipes. Therefore, the net stress states of the pipes tested were used to estimate the cycles-to-leakage of each experiment. However, to account for the effect of mean and multiaxial stresses, the Smith-Watson-Topper criterion was used to determine an equivalent net stress for making cycles-to-leakage estimates (John et al., 2024c; Smith et al., 1970):

$$\sigma_{a,SWT} = \sqrt{\sigma_{n,max}E\varepsilon_{n,a}} \tag{3}$$

where: $\sigma_{a,SWT}$ is the predicted equivalent uniaxial fully-reversed stress amplitude, $\varepsilon_{n,a}$ is the normal strain amplitude on the critical plane (which in the case of linear-elastic multiaxial stress states can be determined using Hooke's law), and the critical plane is that which experiences the maximum value of $\varepsilon_{n,a}$; $\sigma_{n,max}$ is the maximum value of normal stress on the critical plane; and E is the elastic modulus of the material, equal to 82.1 GPa (John et al., 2024b). The equivalent stress amplitude was then used to estimate the cycles-to-leakage of each experiment using the following relationship (Lee, 2005), using the same $\sigma_{A,o}$ and k_0 values as used to calculate F_{an}:

$$N_f = N_A\left(\frac{\sigma_{A,0}}{\sigma_{a,SWT}}\right)^{k_0} \tag{4}$$

The Effective Volume notch fatigue model was developed by Bomas et al. (1999) through combining fracture mechanics theory and a probabilistic approach to the distribution of internal material defects. GCI features many internal inclusions and defects, making the theory behind this model highly relevant. Recent work has shown this model to be effective for GCI pipes featuring circular pits and uniform wall loss, but high-aspect ratio pits have not previously been investigated (John et al., 2026). The Effective Volume model was applied, coupled with the Smith-Watson-Topper criterion, in the following form to make fatigue life estimates:

$$K_{f,ES} = \frac{\sigma_{a,SWT,max}}{\sigma_{a,net}}\left(\frac{V_{eff,SWT,0}}{V_{eff},SWT}\right)^{-1/M_{ES}} \tag{5}$$

Where: $\sigma_{a,SWT,max}$ is the maximum value of the SWT criterion at the notch/pit; $\sigma_{a,net}$ is the net stress amplitude; M_{ES} is a material parameter; $V_{eff,SWT,0}$ is the effective volume of the reference condition in terms the SWT criterion; and $V_{eff,SWT}$ is the effective volume of the condition of interest in terms the SWT criterion. To facilitate calculation using elemental results from FEA, $V_{eff,SWT}$ was approximated as:

$$V_{eff,SWT} = \sum_{i=1}^{n}\left[\left(\frac{\sigma_{a,SWT,i}}{\sigma_{a,SWT,max}}\right)^{M_{ES}}V_i\right] \tag{6}$$

where: n is the number of elements in the FEA model; $\sigma_{a,SWT,i}$ is the SWT equivalent stress amplitude experienced by element i, calculated using Eq. (3); $\sigma_{a,SWT,max}$ is the greatest SWT equivalent stress amplitude experienced by any element in the FEA model; and V_i is the volume of element i. For the cast iron pipes tested, $V_{eff,SWT,0}$ and M_{ES} were found to equal 13,020 mm^3 and 6.90, respectively (John et al., 2026). The cycles-to-leakage of each experiment were estimated using the following relationship:

$$N_f = N_A\left(\frac{[\sigma_{A,0}/K_{f,ES}]}{\sigma_{a,net}}\right)^{k_0} \tag{7}$$

The prediction accuracy of the Net Stress and Effective Volume approaches were quantified using the mean square error quantity, T_{RMS}, as explained by Walat and Łagoda (2014).

FEA was used to calculate the stress quantities needed to determine $K_{t,n}$ and $K_{f,ES}$. This analysis was performed using a quarter pipe model, as shown by Fig. 4a. Considerable mesh refinement was required at the sharp axial pit (see Fig. 4b) to converge the estimate of $K_{f,ES}$, with the resultant minimum element size at the pit tip being 0.028 mm. Full details of the FEA routine used may be found in John et al. (2026), which was similar to that used here with the exception of the pit geometries analysed.

3. Results

3.1. Leak behaviour observations

To investigate the behaviour of early stage leaks, high-speed camera recordings captured the start of leakage for the axial pit experiments featuring internal pressure or biaxial loading. The full leak-to-burst interval of an axial pit-internal pressure load experiment was captured and is shown by Fig. 5 and a video recording provided as supplementary material. The high internal pressure load amplitude applied during this experiment (2.9 MPa) caused the pipe to develop a leaking crack after only 14 load cycles (compared to the target of $>10^3$). This crack grew to the full 20 mm length of the pit during a single load cycle, allowing a jet of water to leak from the crack. However, as the water pressure cycle continued and reduced towards the minimum of 1.2 MPa the leak stopped. This phenomenon is also illustrated for another axial pit-internal pressure load experiment in Fig. 6, where careful comparison of the pressure load history and high-speed video frames showed that leakage only occurred when the internal pressure exceeded approximately its average cyclic value. This stop-start leakage behaviour was observed for all axial pit-internal pressure load and axial pit-biaxial load experiments. In all cases leakage stopped while the internal pressure load was substantially above zero.

Returning to the experiment shown by Fig. 5, after the sudden formation of a leaking crack during load cycle 14 the crack length remained stable for 10 load cycles before suddenly growing beyond the pit during load cycle 23. This crack growth was nearly instantaneous, and the resultant axial crack was over 100 mm long (i.e. over two pipe diameters). This large crack prevented the pipe from holding any water pressure and was therefore considered a burst failure.

The experiment shown by Fig. 5 illustrates the typical leak formation and growth behaviour observed for all axial pit-internal pressure load

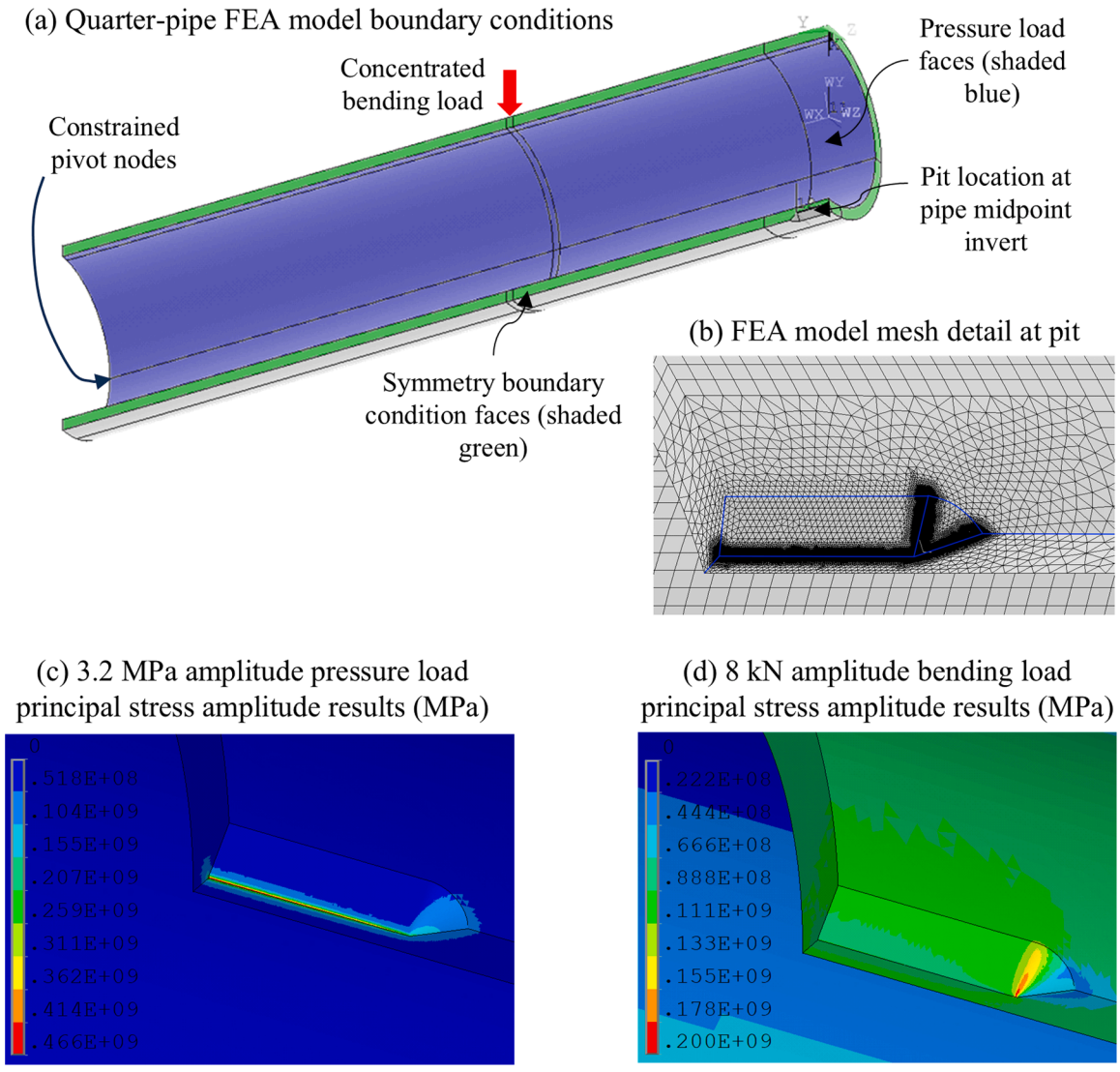

Fig. 4. Illustration of the Finite Element Analysis (FEA) model and boundary conditions (a) and mesh design (b) used to calculate the stress quantities (c, d) required to make fatigue life predictions for test specimens using the Effective Volume notch fatigue model.

and axial pit-biaxial load experiments, however, the number of cycles-to-leakage and leak-to-burst cycles varied considerably across experiments. For example, a lower pressure amplitude experiment (2.3 MPa) where a leaking crack formed after 8167 load cycles is shown by Fig. 7. The initial leaking crack that formed during this experiment was very small, only allowing a bead of water to form at the base of the pit. Over the course of about 150 load cycles this crack grew along the base of the pit until a water jet appeared during the higher-pressure part of the load cycles. The crack continued to grow until it spanned the full width of the pit, however, the crack did not grow beyond the pit despite $>$ 2300 load cycles being applied after the initial leak appeared. The experiment was suspended due to the large quantity of water lost from the system.

The high strength of the axially pitted pipes under bending loading only meant that only one of these specimens developed a leak. The high-speed camera did not trigger successfully when this pipe began to leak, however, measurements of the low water pressure sealed in the pipe during the experiment showed no period of leakage prior to bursting. Instead, a circumferential crack aligned with one end of the pit, shown by Fig. 8, formed during a single load cycle. This leakage and failure behaviour was therefore very different to the axial pit-internal pressure load and axial pit-biaxial load experiments discussed above. All bending load experiments and the uniform wall-loss biaxial experiments developed circumferential cracks upon failure, rather than the axial cracks observed for the axial pit-internal pressure load and axial pit-biaxial load experiments.

3.2. *Leak-to-burst interval*

The leak-to-burst load cycles are plotted against the load cycles taken for a leaking crack to form in Fig. 9, giving a visualisation of the leak stability of each group of experiments. Fig. 9 shows that 19 out of 26 experiments featured some period of leakage prior to the pipe bursting.

Within most groups of experiments there was a trend towards leaks that took more load cycles to form having longer periods of stable leakage prior to bursting. Axial pit–internal pressure load experiments that failed prematurely (i.e. before 10^3 load cycles) are included in Fig. 9 and they illustrate how the trend for this experiment set extends down to lower cycles-to-failure in an almost linear manner within log-log space.

Looking across the different experiment sets in Fig. 9 there are two clear groups, which are highlighted using black and grey markers. The black marker group comprises the axial pit-internal pressure load only and axial pit-biaxial load experiments, and these sets demonstrated periods of stable leakage that were about an order of magnitude greater than the other experiment sets (marked in grey) for similar cycles-to-

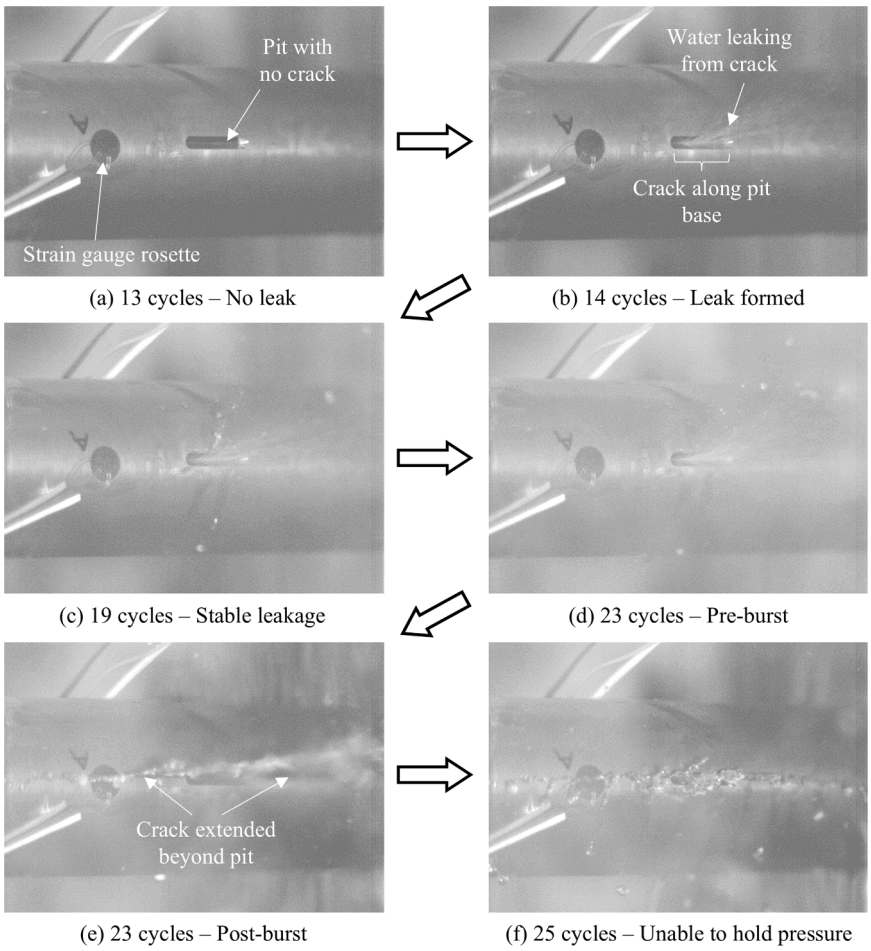

Fig. 5. High-speed video stills showing the development of a leak in a sharp axial notch - internal water pressure experiment with a pressure amplitude of 2.9 MPa and mean pressure of 4.1 MPa. The high loads applied caused the leak to develop quickly, but this meant the high-speed camera was able to capture the full leak-to-burst transition. The initial leaking crack grew to the full length of the 20 mm long pit almost immediately during load cycle 14 (a-b) but then remained stable for 10 load cycles (b-d) before suddenly growing out of the pit to a length of > 100 mm (e), resulting in the pipe bursting. The video from which these stills were taken is provided as supplementary material.

leakage. This indicates that some aspect of the pit-load combination in these two black-marker experiment sets promoted leak stability, rather than the more rapid leak-to-burst transitions observed in the other experiment sets.

3.3. Load cycles-to-leakage for axial pit experiments

Fig. 10 shows the number of load cycles applied before a leaking crack formed vs the applied net stress amplitude for the axial pit experiments. These results were used to investigate the effect of pit-stress alignment on pipe fatigue strength. The net stress amplitude is the equivalent stress amplitude that a pipe with wall thickness uniformly reduced to the depth of the pit would have experienced for the same loading. This means that the net stress can be used to compare the effect of a localised pit with more uniform corrosion. To facilitate this comparison, the 10–90 % prediction interval for pipes with a uniformly reduced wall thickness from John et al. (2024c) are included in Fig. 10. This prediction interval characterises the spread of the uniform wall loss data ($n = 12$).

Only one of the axial pit data points falls within the uniform wall loss prediction interval, indicating that pipes with axial pits were almost always significantly stronger or weaker, depending on the loading, than the uniform wall loss case. This difference from the uniform wall loss case is also quantified by the F_{an} values in Table 3. Two of the axial pit-bending load fatigue experiments survived 10^5 cycles at the maximum load the equipment could apply and were classed as runouts, indicated by the right-pointing arrows on Fig. 10.

Several experiments were performed for the axial pit-internal pressure load experiment set that failed before the threshold 10^3 load cycles, mainly due to the pressure load amplitude being set too high while the behaviour of the pipes was being established. These additional data are plotted in Fig. 11 along with a curve fitted to the data for experiments which leaked after 10^3 load cycles, using the same slope as the unnotched uniaxial data ($k_0 = 11.5$). Surprisingly, given the usual change in fatigue curve slope between the low- and high-cycle fatigue regimes, the curve fits the data well down to a single cycle to failure, except for a single very low strength pipe.

3.4. Fatigue life estimates

To establish whether the observed fatigue strength sensitivity to pit-stress alignment could be predicted by existing models, the cycles to leakage onset predictions made using the Net Stress and Effective Volume methods for the axially pitted pipes are presented in Fig. 12. These prediction plots indicate the effectiveness of the models by comparing the experimentally observed cycles to leakage with the model predictions. Predictions that fall within the parallel chain lines are within the range of expected fatigue strength variation for the pipe material. The T_{RMS} values used to quantify prediction accuracy are provided in Table 4. Some predictions for both methods fell beyond the limits of

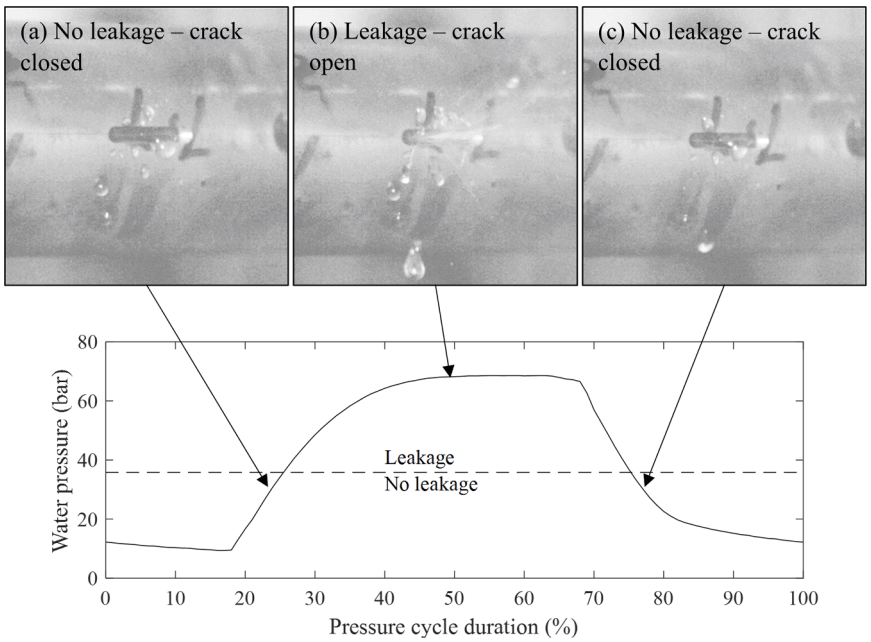

Fig. 6. Example of how leakage only occurred during the higher-pressure part of the load cycles for a sharp axial notch pipe with cyclic internal pressure loading once it had developed a fatigue crack. In image (a) the crack at the base of the pit was closed despite positive internal pressure. Image (b) shows the crack open and leaking due to the increased internal pressure. Image (c) shows the crack closed once again as the pressure dropped. This behaviour repeated each cycle.

expected material variation, indicating that neither method was able to fully capture the effects of different pit-stress alignments.

4. Discussion

4.1. Intermittent leakage behaviour of fatigue cracks

A particularly striking and novel observation made by this research was the stop-start leakage behaviour of the fatigue cracks formed during the axial pit-internal pressure loading and axial pit-biaxial loading experiments. In all of these experiments leakage began once a fatigue crack a few mm long penetrated through the pipe's wall. However, when the cyclic pressure load dropped below approximately the middle value the crack closed and leakage stopped (Fig. 6).

This observation is perhaps surprising given that the applied pressure loads were around ten times greater than those experienced by pipes in service, meaning the crack was able to close despite the applied pressure being extremely high. John et al. (2024c) found that normal strain amplitude (i.e. crack opening) controls fatigue crack growth in grey cast iron. This means that a lower pressure load which causes a crack to form must be able to cause sufficient strain to open the crack, and therefore leakage should be possible for some part of the loading cycle. This stop-start leakage behaviour is likely to only apply to newer, smaller cracks because erosion may increase the crack width over time, whilst long cracks may cause sufficient global plastic deformation during their formation such that they cannot close.

Fatigue crack closure, where at least the tips of a fatigue crack have been found to remain closed for portions of tensile load cycles, has been encountered in other engineering applications including aircraft aluminium alloys and steel railway axles (Pokorny et al., 2017; Wallbrink et al., 2023). In these cases, crack closure is important because it affects crack growth rate. The mechanisms used to explain such crack closure observations include: plastic deformation; oxidation of the crack faces; crack face surface roughness; and fretting debris (Janssen et al., 2004; Pokorny et al., 2017). Recent work has successfully measured crack opening displacement in 4 mm diameter ductile iron specimens using X-ray tomography, detecting plasticity-induced crack closure near the tips of a ~1 mm crack at 37 % of the maximum tensile load (Xiao et al., 2024). In the present research, crack closure has been inferred through the cessation of leakage below about 50 % of the maximum tensile load, implying that the crack closure mechanism affected the full 20 mm crack length, not just the crack tips, which merits future detailed investigation.

The observation that small through-wall fatigue cracks may close and completely stop leaking while internal water pressures are above zero has significant implications for leak detection techniques, WDN pressure management, and WDN hydraulic modelling. Leak detection techniques to search for this type of small leaking crack in GCI pipes should be used during the times of day when the network water pressure is high to increase the likelihood of the leak being open and detectable, assuming the leaks were caused by an internal pressure load. Acoustic and vibration leak detection is commonly conducted at night when background noise is minimal and pressures are typically higher, complying with this. Similarly, night line estimation from DMA flow meters is typically when pressures are highest, so is likely to quantify the worst effects of such small leaks in GCI pipes. This behaviour can also explain the benefits of pressure management, and inform pressure reduction targets: a substantial, non-linear reduction in leakage should theoretically be achieved in WDNs containing GCI pipes with large numbers of small leaking fatigue cracks by reducing the operating pressure such that the cracks are unable to open.

The finding that small fatigue cracks can stop leaking completely under positive water pressures potentially gives physical meaning to the negative initial leak areas calculated by Deyi et al. (2014) for a real water network using the "Fixed and Variable Area Discharges" pressure-leakage relation. A negative initial leak area in such analysis results in zero leakage being predicted below some positive value of water pressure, while using a positive initial leak area predicts that leakage occurs at zero pressure. Instead of being impossible, negative initial leak areas may indicate a significant proportion of the leakage water loss from the WDN is caused by small fatigue cracks that are able to close, assuming the WDN in question contains many GCI pipes. Such variable area effects were observed for plastic pipes by Fox et al. (2016), however not to the extent of causing zero leakage. This is likely due to removing material to formation the slits in the prior work.

Inferring the existence and location of small leaking fatigue cracks in

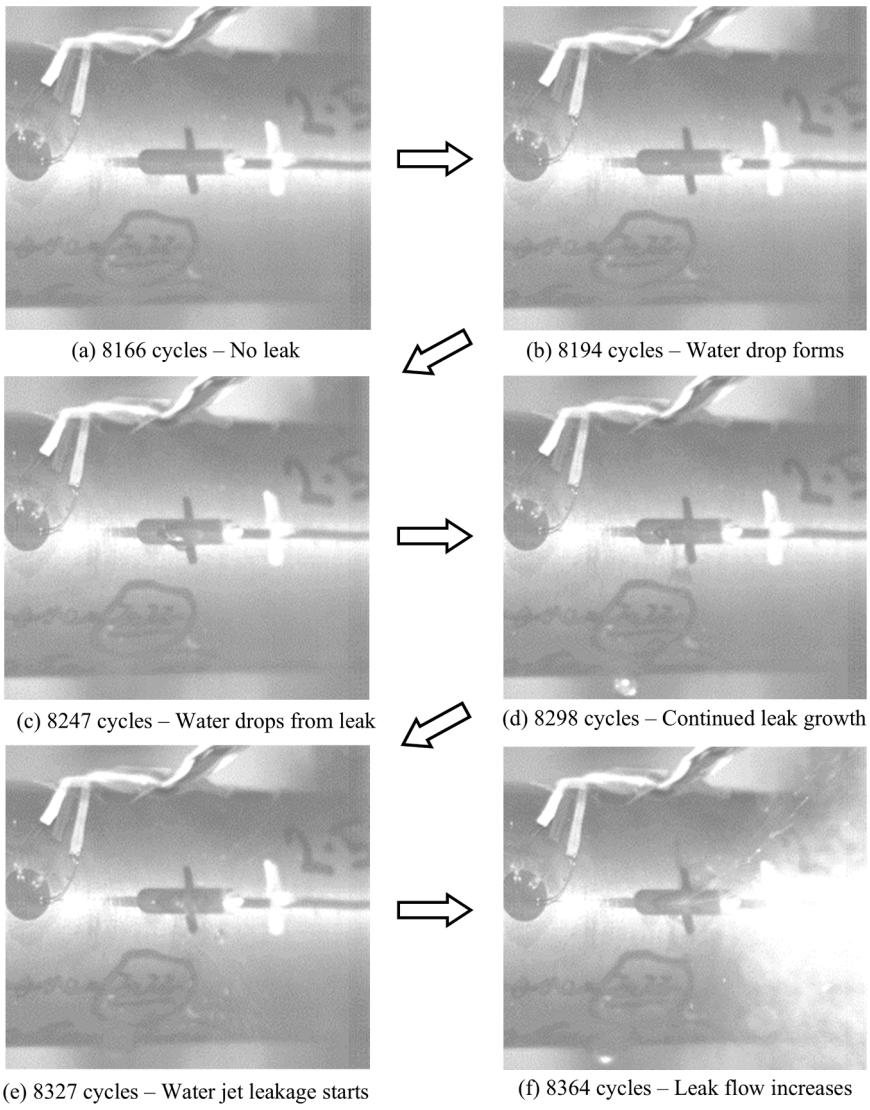

Fig. 7. High-speed video stills showing the development of a leak in a sharp axial notch - internal water pressure experiment. Leakage began after 8167 cycles (a-b) when a tiny water drop began to form at the bottom of the pit, showing a crack had formed. The leak developed slowly, first allowing water to drip from the crack (c-d), then growing to allow water to jet out(e-f). The crack eventually grew to the full width of the pit, but the experiment was suspended without bursting after 10,565 cycles due to the quantity of water loss from the system.

Fig. 8. Image showing the circumferential crack alignment of the only axial pit pipe that failed due to cyclic bending loading. Note that the crack passes through one end of the pit, rather than the centre.

GCI pipes using hydraulic modelling approaches is likely to be inaccurate if the crack closure behaviour observed in this study is not modelled accurately. Experiments used to validate pressure-leakage behaviour models often approximate cracks in pipes as having a small finite width (~ 1 mm) due to specimen manufacture constraints (Fox et al., 2016; Li et al., 2022; Van Zyl and Malde, 2017), however, non-zero width cracks do not display the crack closure behaviour observed in this study.

4.2. *Effect of pit-stress alignment on the leak-to-burst interval*

It was hypothesised that pit-stress alignment can cause a significant change in the leakage behaviour of GCI pipes. This hypothesis is supported by the leak-to-burst interval results in Fig. 9 which show that the axial pit-internal pressure load and axial pit-biaxial load experiment sets demonstrated periods of stable leakage that were about an order of magnitude longer (in terms of applied load cycles) than the other experiment sets.

The axial pit-internal pressure load and axial pit-biaxial load were also the most "damaging" pit configurations, causing leaks to form at lower applied stress amplitudes. F_{an} for the sharp and blunt round pit specimens were 0.77 and 0.74, respectively (John et al., 2026), whereas F_{an} for axial pit-internal pressure load and axial pit-biaxial load experiments were higher at 1.40 and 1.60, respectively (Table 3). The higher F_{an} values show that the axial pit-internal pressure load and axial pit-biaxial load configurations allowed leaking cracks to form under lower loads, meaning that stresses in the iron surrounding the pits were lower relative to the stresses at the bottom of the pit where the cracks formed in these cases.

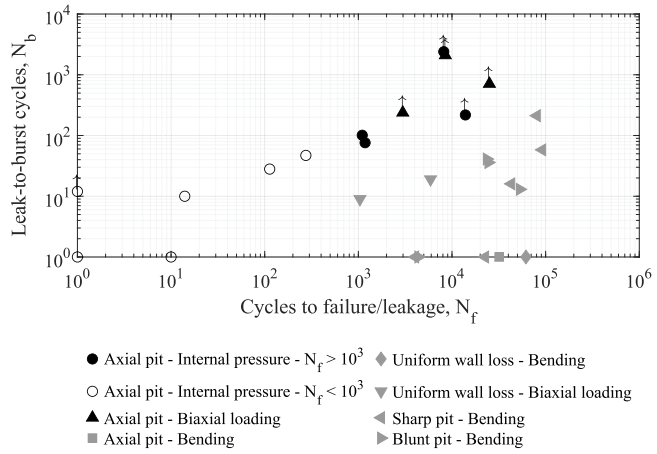

Fig. 9. Plot of the number of load cycles to leakage vs number of cycles between leakage starting and structural failure of the specimen. Upward arrows indicate that an experiment was suspended before unstable crack propagation occurred.

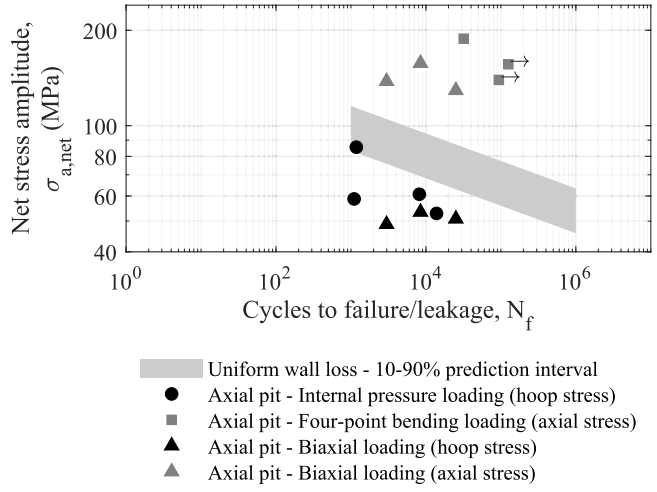

Fig. 10. Plot showing the fatigue life results for pipe specimens featuring axial pits subjected to internal pressure, bending, or combined bending and internal pressure loads (i.e. biaxial loading). The legend indicates the direction of the stress amplitude shown for each data set. The expected range of fatigue strengths for pipes with uniform wall loss subjected to $R = 0.1$ uniaxial loading (John et al., 2024c) is provided for reference.

The substantial difference in stress state between the bottom of the axial pit and surrounding iron likely caused the crack propagation behaviour shown in Figs. 5 and 7. In both figures, the crack was observed to grow relatively quickly in the high-stress region at the base of the pit. However, crack growth slowed considerably once the crack tips reached the significantly lower stress region at the edge of the pit. The pit was able to arrest crack growth and "trap" the crack for a period. On the other hand, for the lower stress concentration pit-stress configurations the difference in stresses between the bottom of the pit and the surrounding iron were small, meaning the crack was able to grow beyond the pit with greater ease, resulting in the shorter leak-to-burst intervals observed. Similarly, the short leak-to-burst intervals of the uniform wall loss experiments were also likely due to the more uniform stresses providing a good environment for crack growth.

The critical crack length for unstable crack propagation (or burst in this case) can be estimated using the Linear Elastic Fracture Mechanics relation for a through-thickness crack in an infinite plate (Janssen et al., 2004):

$$a_{cr} = \frac{1}{\pi}\left(\frac{K_{IC}}{\sigma_n}\right)^2 \tag{8}$$

Where K_{IC} is the material fracture toughness, typically close to 13.8 MPa$\sqrt{m}$ for spun GCI pipes (Makar and Rajani, 2000), and σ_n is the stress applied perpendicularly to the crack. For the axial pit-internal pressure experiments that developed leaks after between 10^3 and 10^4 cycles, the predicted critical total crack length, $2a_{cr,gross}$, was about 34 mm (given the maximum gross stress was approximately 60 MPa). Considering that the length of the sharp axial notches was 20 mm, this estimated critical crack length indicates that in this loading condition a critical crack could not form in the high-stress region at the base of the sharp axial notch, as illustrated by Fig. 13a. If the sharp axial notch length had been 34 mm, or more, it is unlikely that extended periods of stable leakage would have occurred because a critical crack would have been able to form in the high-stress region of the notch, as illustrated by Fig. 13b This is supported by the observation of rapid propagation of small cracks in the uniform wall loss experiments reported here, and some experiments using ramped internal pressures reported by Rathnayaka et al. (2017), where there were no barriers to crack propagation. Further experiments exploring the leak-to-burst interval would be

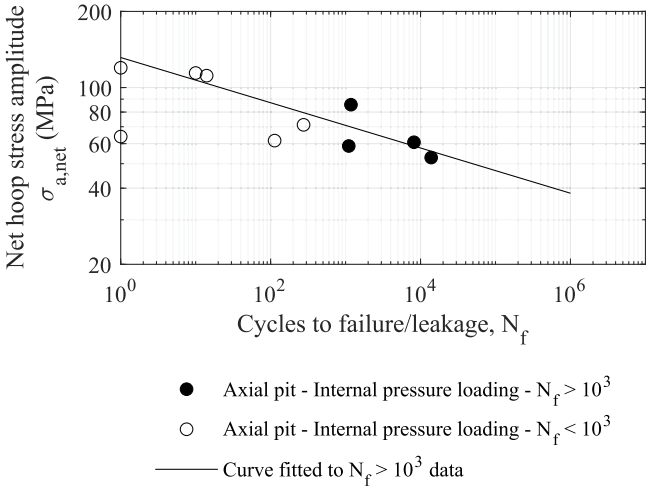

Fig. 11. Plot showing all axial pit pipe internal pressure loading fatigue data, including failures that occurred before 10^3 cycles. The curve shown was fitted using only data corresponding to failures after 10^3 cycles, showing that the same linear trend persists to very low cycles to failure.

Table 3
Fatigue experiment parameters and quantification of the fatigue strength demonstrated relative to the uniform wall loss case via the parameter F_{an} (see Eq. (2)).

Loading	Experiments	Runouts	Average load ratio, R	$K_{t,g}$	$K_{t,n}$	F_{an} ± 90 % confidence interval
Internal pressure	4	0	0.16	18.93	7.63	1.40 ± 0.26
Bending	3	2	0.10	2.44	1.23	< 0.56
Biaxial*	3	0	0.23 / 0.18	2.29 / 17.93	1.15 / 7.23	0.84 ± 0.16 / 1.60 ± 0.33

* R, $K_{t,g}$, $K_{t,n}$ and F_{an} values for: axial stress / hoop stress.

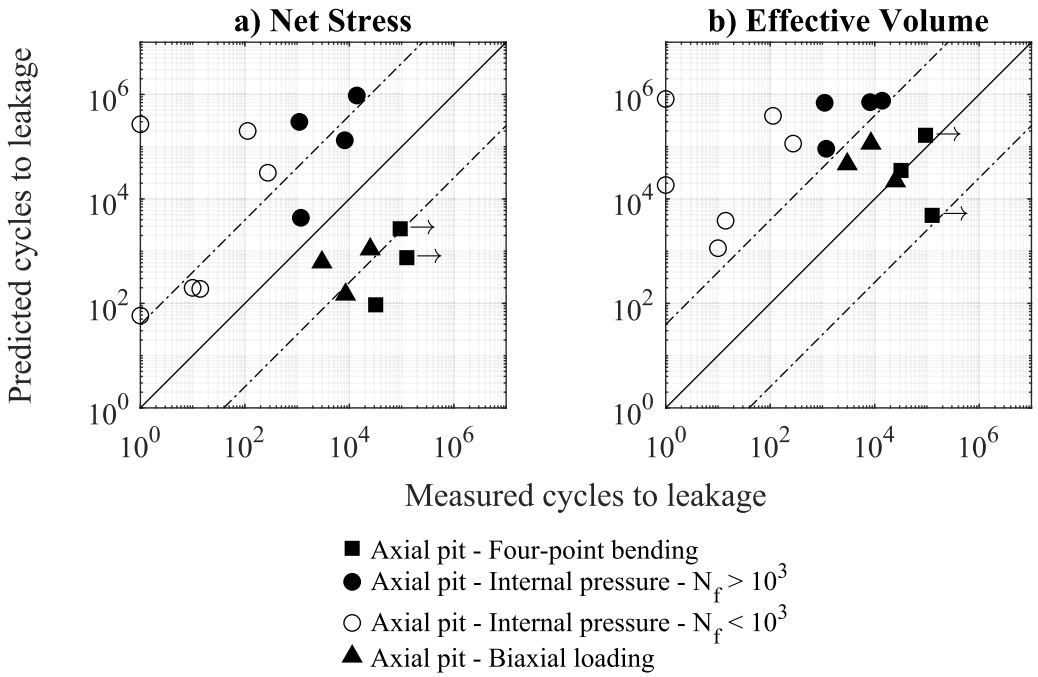

Fig. 12. Plots comparing the cycles to leakage predictions of the (a) Net Stress and (b) Effective Volume methods with the cycles to leakage measured during the experiments. The solid line indicates perfect prediction, whereas the chain lines indicate the observed scattering of the pipe material under uniaxial fully-reversed fatigue loading (John et al., 2024c).

Table 4
Quantification of the cycles to failure prediction errors using the T_{RMS} parameter.

	Prediction error, T_{RMS}		
	Axial pit – Four-point bending loading	Axial pit – Internal pressure loading	Axial pit – Biaxial loading
Net Stress	339.2	46.2	22.0
Effective Volume	1.1	135.5	8.9

beneficial to confirm this behaviour for a wide range of real-world corrosion pit geometries.

This mechanism whereby cracks can become "trapped" in smaller, high stress concentration pits explains how small, difficult to detect leaks can form and persist for extended periods of time without propagating to form a larger leak or burst. If a crack that has been "trapped" by a corrosion pit in this way results in a leak that is too small to detect, then the crack would contribute to the "background" leakage rate of a WDN until it is able to propagate beyond the pit, which may then enable the leak to be detected.

The finding that pit shape influences crack stability also creates the potential for in-pipe inspection tools to identify pipes at risk of developing "background" leaks from corrosion pit measurement data. Further research into the relation between pit shape leak stability could ultimately enable asset managers in possession of corrosion pit measurements and stress predictions for in-service GCI pipes to determine the likelihood of the pipe developing a stable leak or a more sudden burst.

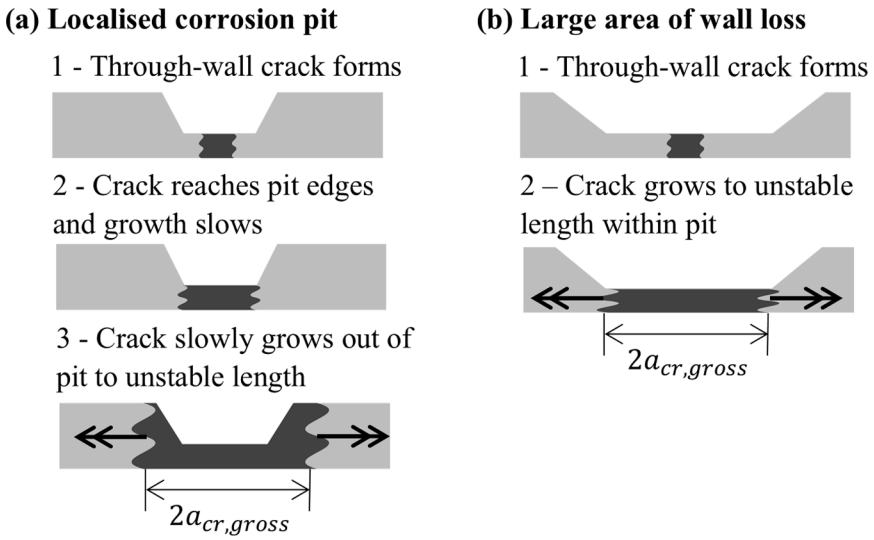

Fig. 13. Illustration of the proposed interaction between corrosion pit size and critical fatigue crack length, showing how pits less than the critical crack length may "trap" cracks for a period. Double arrows indicate rapid, unstable crack propagation, leading to burst.

Direct comparison of these experimental leak-to-burst interval results to real-world case studies requires knowledge of the frequency of the load which caused the real-world leak, however loading frequency information is rarely recorded or reported for specific leak-to-burst examples. Load cycle frequencies can vary significantly: internal pressure load cycle frequencies may range between perhaps one per year for extreme events to 10^5 per year for more minor instabilities (Jara-Arriagada and Stoianov 2022; Jiang et al., 2019). For an experimental internal pressure load result of 200 leak-to-burst cycles the real-world leak-to-burst time could therefore potentially vary between several years to less than a day. Stephens et al. (2020) observed a longitudinal crack that had a detectable leak-to-burst period of about 6 months; hypothetically, 200 load cycles over this period would correspond to a load frequency of 400 per year, which is within the range of plausible pressure load frequencies.

4.3. *Effect of pit-stress alignment on fatigue strength*

The second aspect of this research's hypothesis was that different corrosion pit and stress axes alignments cause a significant change in the fatigue strength of GCI pipes. High aspect ratio pits were tested because these were expected to be most sensitive to pit-stress alignment changes.

So that these findings can easily be transferred to operational load magnitudes (from the higher load magnitudes applied during the experiments) the discussion in this section refers to percentage changes in net fatigue strength at the high-cycle reference cycles to leakage (10^6). Net stress in pipes is a function of load magnitude and remaining wall thickness and is linked to the local stresses that control the fatigue damage process. Different combinations of load and wall thickness can return the same net stress amplitude and therefore similar cycles to leakage (i.e. a lower, operational load and lower remaining wall thickness could return the same number of cycles to failure as a given experiment if the net stress amplitudes and pit shapes are equal). The net stress amplitude is therefore a useful comparative quantity as it is not constrained to a particular load magnitude.

The effect of pit-stress alignment for the axially pitted pipes is shown by Fig. 10. Directly comparing the results for the axial pit-internal pressure load experiments and axial pit-bending load experiments in Fig. 10 shows that rotating the applied stress direction through 90° from parallel to the pit axis to perpendicular (see Fig. 1d and f) reduced the fatigue strength of the pipes by about 60 %. This shows that high aspect ratio corrosion pits can be highly sensitive to stress direction, as hypothesised. This effect was caused by the asymmetry of the pit amplifying stresses applied in different directions to varying degrees, seen by comparing the K_t values in Table 3. This means that if a GCI pipe features high aspect ratio corrosion pits, such as the examples reported by Jara-Arriagada and Stoianov (2024) and Makar (2000), changes in the pipe loading may cause the pit to become substantially more, or less, damaging.

To illustrate the way in which a change in loading may cause a pit to become more damaging, and how the results obtained using axially aligned pits can be translated to circumferentially aligned pits, consider the following example. A long narrow pit aligned *circumferentially* is a 90° rotation of the *axial* pits tested in this research, so a circumferential pit would amplify the effect of axial stresses and be relatively insensitive to hoop stresses. Therefore, a circumferentially aligned pit would cause little reduction in fatigue strength when internal water pressure loading is applied, however, if a cyclic bending load were subsequently introduced, perhaps due to fluctuations in soil moisture content (Chan et al., 2015), the pit would amplify the axial stresses caused by this load which could lead to a leak forming in a short space of time.

Comparing the axial pit results with the uniform wall loss case shows that all-but-one of the axial pit-internal pressure load data in Fig. 10 fell below the uniform wall loss prediction interval. This shows the axial pit-internal pressure load configuration was typically more damaging than the uniform wall loss case, as quantified by the F_{an} value of 1.40 given in Table 3 (i.e. a 29 % reduction in fatigue strength). The 90 % confidence interval for this F_{an} value is ± 0.26 due to the scatter in results and small amount of data, however, *t*-test results showed that the difference between these two data sets was significant to a > 95 % confidence level. Therefore, the damaging effect of the axial pit-internal pressure load configuration can be considered significant but additional tests, perhaps with a realistic irregular pit geometry, would be beneficial to quantify the effect with greater certainty.

On the other hand, all the axial pit-bending load data fell considerably above the uniform wall loss prediction interval, showing this configuration was less damaging than the uniform wall loss case. Although only one axial pit-bending load experiment developed a leak, the number of cycles survived by the other two experiments indicate that they would likely have demonstrated similar, or higher, fatigue strengths. This means the F_{an} value of 0.56 for this dataset (i.e. a 79 % *increase* in fatigue strength) can only be considered an approximate value. Critically, for both the parallel and the perpendicular stress-pit axis alignments (see Fig. 1d and f) the axially pitted pipes gave substantially different fatigue strengths than the uniform wall loss case.

An implication of the above finding is that modelling complex corrosion pit geometries as uniform wall loss (a relatively common industry practice) has the potential to significantly overestimate or underestimate a GCI pipe's strength. This in turn may result in wasted resources due to pipes being replaced prematurely, or water loss due to pipes developing leaks earlier than expected.

Considering the effect of biaxial loading, the axial pit-biaxial load experiments behaved similarly to the internal pressure load experiments, making it appropriate to analyse these experiments from a hoop-stress perspective. The addition of the out-of-phase bending load caused a further average reduction of fatigue strength by 12 % relative to the internal pressure load only ($F_{an} = 1.60$), however *t*-test results showed this difference was not significant to a 90 % confidence level. This reduction is also less than the 28 % strength reduction reported by John et al. (2026) for uniform wall loss pipes subjected to out-of-phase biaxial loading. This indicates that GCI pipes with larger areas of uniform wall loss corrosion may be more vulnerable to combined loads than pipes with smaller pointed pits.

The above findings are derived from experiments using machined pits causing $K_{t,n}$ from 1.23 to 7.63, depending on the loading condition. The low sensitivity of cast iron to surface roughness (Lampman, 1996) and the low strength of graphitic corrosion residue (Seica and Packer, 2004; Yamamoto et al., 1983) mean these machined pits are expected to cause similar fatigue strength reductions to real corrosion of the same shape, although it is unlikely such regularly shaped pits would occur in reality. The parameter $K_{t,n}$ quantifies the severity of the geometric stress concentration effect of different pits, which appears to correlate with the fatigue strength reduction caused by a pit (John et al., 2026). As a result, real pits causing a similar $K_{t,n}$ to the machined pits are likely to cause a similar magnitude fatigue strength reduction. However, $K_{t,n}$ has rarely been quantified for real corrosion pit geometries; a small number of studies have performed FEA using 3D scans of corroded cast iron and steel pipe geometries with internal pressure loads (Mokhtari and Melchers, 2020; Rathnayaka et al., 2017), the results of which suggest $K_{t,n}$ values of between about 0.8 and 3.2. The small number of real corrosion patches investigated in this way mean this range cannot be considered comprehensive and images of corrosion pits available in the literature suggest that higher $K_{t,n}$ pits are likely to exist (Jara-Arriagada and Stoianov 2024; Makar, 2000). To understand the full range of fatigue strength reductions caused by real corrosion pits, it would be beneficial to perform a large-scale campaign of exhumed pipe corrosion pit scanning and fatigue analysis using the understanding developed by this research.

4.4. Predicting the effect of pit-stress alignment on fatigue strength

Given that the cycles-to-leakage results in Fig. 10 show that pit-stress alignment can significantly change the fatigue strength of a GCI pipe it is important to understand whether this change in fatigue strength can be predicted. Looking to the fatigue life estimates, the Net Stress method (Fig. 12a) underestimated the fatigue life of the axial pit-bending load experiments, showing that this model did not capture the lower damage caused by this configuration. Similarly, the Net Stress model did not capture the increased damage caused by the axial pit-internal pressure load configuration and overestimated the lives of these experiments. The lives of the axial pit-biaxial load experiments were slightly underestimated, suggesting that the damaging effect of the out-of-phase biaxial load was over-accounted for. The relatively poor performance of the Net Stress method was not unexpected, given this method assumes the pits behave as uniform wall loss.

The Effective Volume method (Fig. 12b) provided reasonable predictions for the axial pit-bending and axial pit-biaxial experiments, although one of the runout bending experiments would probably have been underestimated had the experiment continued to failure. This suggests the method broadly captured the effect of the pit-stress alignments in these configurations. Surprisingly, given the good biaxial experiment predictions, the Effective Volume method provided worse predictions for the axial pit-internal pressure load experiments than the Net Stress method (note the higher T_{RMS} value in Table 4), with all predictions overestimating the cycles to leakage beyond the material scatter band. This indicates that the Effective Volume method did not capture the damaging effect of the perpendicular pit-stress alignment, which suggests that the good biaxial experiment predictions noted above may have been driven by overestimation of the biaxial load effect. Previously, the Effective Volume approach has been applied to pits characterised by a net stress concentration factor of 4.5 or less (John et al., 2026), compared to over 7 in this research. As a result, further research is needed to understand and predict the notch fatigue behaviour of GCI pipes featuring high stress concentration pits. Additional fatigue experiments of pipes with a range of realistic pit geometries would be invaluable in developing an improved model.

The cycles-to-leakage results for the axial pit-internal pressure load configuration that developed leaks after between 1 and 10^3 load cycles are surprising because a change in the slope of the fatigue curve would be expected in this region (Carpinteri et al., 2017; Fatemi and Shamsaei, 2011). Instead, Fig. 11 shows that the curve fitted to the high-cycle fatigue data ($N_f > 10^3$) also fits the low-cycle fatigue data well. This may be because the high stress concentration effect of the axial pit in this configuration meant that crack development occurred in plastic strain conditions even when N_f was greater than 10^3, meaning there was no change in cracking mode as N_f reduced. This implies that it may be possible to use a single unifying linear-elastic model to predict static (i.e. $N_f = 1$), low-cycle fatigue, and high-cycle fatigue failures for pitted GCI pipes, which could simplify failure prediction significantly once a suitable model is identified or developed.

5. Conclusions

The research presented in this paper explored the hypothesis that different corrosion pit and multiaxial stress alignments cause a significant change in the fatigue strength and leakage behaviour of grey cast iron pipes. The conclusions reached are:

- Leaking fatigue cracks in grey cast iron pipes can close and stop leaking when the load that caused the crack to form is reduced below about the middle cyclic value. This means that leaks may disappear (even under high pressure conditions) and subsequently reappear as the loading applied to a pipe changes.
- Leaking cracks that take more load cycles to develop tend to have longer periods of stable leakage prior to bursting, provided conditions do not change.
- Small corrosion pits that cause high stress concentrations can cause leak-to-burst intervals that are two orders of magnitude longer than uniform wall loss because they restrict crack propagation.
- The common practice of assuming corrosion pitting equates to uniform wall loss can result in significant over- or under-estimates of fatigue strength for cast iron pipes, particularly for those featuring long, narrow pits.
- The fatigue strength reduction caused by long, narrow corrosion pits can change by about 60 % depending on the applied stress direction. Therefore, to evaluate the damage caused by specific corrosion pits it is important to understand the loads experienced by a pipe.
- The Effective Volume notch fatigue model can underestimate the damaging effect of pit and load combinations that cause high net stress concentrations of around 7.
- The fatigue behaviour of pitted cast iron pipes does not show a clear transition between the low- and high-cycle fatigue regimes, suggesting that linear elastic fatigue analysis may be applicable to fatigue lives from 1 to $> 10^5$ cycles. This would significantly simplify failure analysis of these pipes.

Funding

This research was funded by UK Water Industry Research (UKWIR) and the Engineering and Physical Sciences Research Council (EPSRC) through the Water Infrastructure and Resilience (WIRe) Centre for Doctoral Training (EPSRC funding reference: EP/S023666/1).

CRediT authorship contribution statement

E.D.A. John: Writing – original draft, Methodology, Investigation, Formal analysis. **J.B. Boxall:** Writing – review & editing, Methodology, Funding acquisition, Conceptualization. **R.P. Collins:** Writing – review & editing, Methodology, Funding acquisition, Conceptualization. **E.T. Bowman:** Writing – review & editing, Methodology, Funding acquisition, Conceptualization. **L. Susmel:** Writing – review & editing, Project administration, Methodology, Funding acquisition, Conceptualization.

Declaration of competing interest

The authors declare that they have no known competing financial interests or personal relationships that could have appeared to influence the work reported in this paper.

Acknowledgements

The authors would like to thank Dennis Dellow and Jeremy Heath from UKWIR for bringing an experienced industry perspective to the project. The authors give a special thanks to the University of Sheffield technicians Paul Blackbourn, Richard Kay, Martin Taylor, Mario Dorna, Sam Gibson, Kieran Nash, Kieren Howarth, and Paul Bentley for their invaluable work and assistance. For the purpose of open access, the author has applied a Creative Commons Attribution (CC BY) licence to any Author Accepted Manuscript version arising from this submission.

Supplementary materials

Supplementary material associated with this article can be found, in the online version, at doi:10.1016/j.watres.2026.126046.

Data availability

The research data produced is available at the following repository: https://doi.org/10.15131/shef.data.31073086.

References

Anglian Water, 2024. Price review 2024 (PR24) business plan tables (version 7) [data tables]. https://www.anglianwater.co.uk/siteassets/household/about-us/pr24/dd/anh_dd_004-v7-main-data-tables.xlsb.

Atkinson, K., Whiter, J.T., Smith, P.A., Mulheron, M., 2002. Failure of small diameter cast iron pipes. Urban Water. 4, 263–271. https://doi.org/10.1016/S1462-0758(02)00004-3.

Barton, N.A., Farewell, T.S., Hallett, S.H., Acland, T.F., 2019. Improving pipe failure predictions: factors affecting pipe failure in drinking water networks. Water. Res. 164, 114926. https://doi.org/10.1016/j.watres.2019.114926.

Bomas, H., Linkewitz, T., Mayr, P., 1999. Application of a weakest-link concept to the fatigue limit of the bearing steel SAE 52100 in a bainitic condition. Fatigue Fract. Eng. Mater. Struct. 22 (9), 733–741. https://doi.org/10.1046/j.1460-2695.1999.t01-1-00211.x.

Boxall, J.B., O'Hagan, A., Pooladsaz, S., Saul, A.J., Unwin, D.M., 2007. Estimation of burst rates in water distribution mains. Proc. Inst. Civ. Eng. 160 (WM2), 73–82. https://doi.org/10.1680/wama.2007.160.2.73.

Brevis, W., Susmel, L., Boxall, J., 2015. Investigating in-service failures of water pipes from a multiaxial notch fatigue point of view: a conceptual study. Proc. Inst. Mech. Eng. C 229 (7). https://doi.org/10.1177/0954406214553020.

British Standards Institution, 1990. Discharge and Ventilating Pipes and fittings, Sand-Cast Or Spun in Cast Iron - Part 2: Specifications for Socketless Systems. British Standards Publications. BS 416-2:1990.

British Standards Institution, 1958. BS 1211:1958 Centrifugally Cast (Spun) Iron Pressure Pipes For water, Gas & Sewage. British Standards Publications, London.

Carpinteri, A., Spagnoli, A., Vantadori, S., 2017. A review of multiaxial fatigue criteria for random variable amplitude loads. Fatigue Fract. Eng. Mater. Struct. 40 (7), 1007–1036. https://doi.org/10.1111/ffe.12619.

Chan, D., Gallage, C.P.K., Rajeev, P., Kodikara, J., 2015. Field performance of in-service cast iron water reticulation pipe buried in reactive clay. Can. Geotech. J. 52, 1861–1873. https://doi.org/10.1139/cgj-2014-0531.

Deyi, M., Van Zyl, J., Shepherd, M., 2014. Applying the FAVAD concept and leakage number to real networks: a case study in Kwadabeka, South Africa. Procedia Eng. 89, 1537–1544. https://doi.org/10.1016/j.proeng.2014.11.450.

Dwr Cymru, 2024. Price review 2024 (PR24) business plan tables (version 7) [data tables]. https://corporate.dwrcymru.com/-/media/project/files/page-documents/corporate/library/pr24-reports/august-2024/2-data-tables/wsh-dd-101-pr24-business-plan-tables-v7.ashx.

Elmrom, T.A.A, 2021. Impact of Voids on Buried Utility Pipes Subjected to Surface Traffic Loading. University of Sheffield [PhD. https://etheses.whiterose.ac.uk/id/oai_id/oai:etheses.whiterose.ac.uk:31464.

Fahimi, A., Evans, T.S., Farrow, J., Jesson, D.A., Mulheron, M.J., Smith, P.A., 2016. On the residual strength of aging cast iron trunk mains: physically-based models for asset failure. Mater. Sci. Eng. A 663, 204–212. https://doi.org/10.1016/j.msea.2016.03.029.

Fatemi, A., Shamsaei, N., 2011. Multiaxial fatigue: an overview and some approximation models for life estimation. Int. J. Fatig. 33 (8), 948–958. https://doi.org/10.1016/j.ijfatigue.2011.01.003.

Folkman, S., 2018. Water main break rates In the USA and Canada: a comprehensive study. https://digitalcommons.usu.edu/.

Fox, S., Boxall, J., Collins, R., 2018. Derivation and validation of a leakage model for longitudinal slits in polyethylene pipes. J. Hydraul. Eng. 144 (7), 04018034. https://doi.org/10.1061/(ASCE)HY.1943.

Fox, S., Collins, R., Boxall, J., 2016. Experimental study exploring the interaction of structural and leakage dynamics. J. Hydraul. Eng. 143 (2), 04016080. https://doi.org/10.1061/(ASCE)HY.1943-7900.0001237.

Fu, G., Zhang, C., Deo, R., Rathnayaka, S., Shannon, B., Kodikara, J., 2023. A model of stress concentration factors for external corrosion patches on large-diameter underground cast iron pipes. Sustain. Resilient. Infrastruct. 8 (1), 109–120. https://doi.org/10.1080/23789689.2020.1828022.

He, M., Li, J., Liu, Y., Tang, X., 2026. Water pipe leakage detection method based on bi-sensor data fusion. Water. Res. 288, 124697. https://doi.org/10.1016/j.watres.2025.124697.

Janssen, M., Zuidema, J., Wanhill, R.J.H, 2004. Fracture mechanics: Fundamentals and Applications, 2nd ed. Taylor & Francis Group.

Jara-Arriagada, C., Stoianov, I., 2022. High resolution water pressure monitoring for the assessment of fatigue damage in water pipes. In: 2nd International Joint Conference on Water Distribution Systems Analysis and Control in the Water Industry. https://doi.org/10.4995/WDSA-CCWI2022.2022.14813. Valencia.

Jara-Arriagada, C., Stoianov, I., 2024. Pressure-induced fatigue failures in cast iron water supply pipes. Eng. Fail. Anal. 155, 107731. https://doi.org/10.1016/j.engfailanal.2023.107731.

Jiang, R., Rathnayaka, S., Shannon, B., Zhao, X.L., Ji, J., Kodikara, J., 2019. Analysis of failure initiation in corroded cast iron pipes under cyclic loading due to formation of through-wall cracks. Eng. Fail. Anal. 103, 238–248. https://doi.org/10.1016/j.engfailanal.2019.04.031.

John, E., Boxall, J., Collins, R., Bowman, E., Susmel, L., 2024a. Experimental investigation of the fatigue strength and leakage failure mode of corroded cast iron water pipes. Eng. Proc. 69 (1), 20. https://www.mdpi.com/2673-4591/69/1/20.

John, E., Boxall, J., Collins, R., Bowman, E., Susmel, L., 2024b. Fatigue failure analysis of grey cast iron water pipes accounting for fatigue strength variation. Eng. Fail. Anal. 165, 108762. https://doi.org/10.1016/j.engfailanal.2024.108762.

John, E., Boxall, J., Collins, R., Bowman, E., Susmel, L., 2024c. Multiaxial fatigue of water pipe grey cast iron. Int. J. Fatig. 178, 108002. https://doi.org/10.1016/j.ijfatigue.2023.108002.

John, E.D.A., Boxall, J.B., Collins, R.P., Bowman, E.T., Susmel, L., 2025. An experimental method for fatigue testing cast iron water pipes using combined internal water pressure and bending loads. Exp. Mech. https://doi.org/10.1007/s11340-025-01153-6.

John, E.D.A., Boxall, J.B., Collins, R.P., Bowman, E.T., Susmel, L., 2026. Multiaxial notch fatigue of corroded cast iron pipes. Int. J. Fatig. 202. https://doi.org/10.1016/j.ijfatigue.2025.109247.

Lampman, S. (1996). Fatigue and fracture properties of cast irons. In ASM Handbook, Vol. 19: Fatigue and Fracture (pp. 665–679). https://doi-org.sheffield.idm.oclc.org/10.31399/asm.hb.v19.a0002399.

Lee, Y.L., 2005. Fatigue Testing and analysis: Theory and Practice, 1st ed. Elsevier Science & Technology.

Li, Y., Gao, J., Shen, C., Guan, Y., Wang, W., 2022. Estimation of leak area-pressure relationship for cracks on water pipes using models based on linear-elastic fracture mechanics. Water. Res. 221, 118692. https://doi.org/10.1016/j.watres.2022.118692.

Logan, R., Mulheron, M.J., Jesson, D.A., Smith, P.A., Evans, T.S., Clay-Michael, N., & Whiter, J.T. (2014). Graphitic corrosion of a cast iron trunk main: implications for asset management WIT transactions on the built environment, Vol 139, doi:10.2495/UW140351.

Makar, J.M., 2000. A preliminary analysis of failures in grey cast iron water pipes. Eng. Fail. Anal. 7, 43–53. https://doi.org/10.1016/S1350-6307(99)00005-9.

Makar, J.M., Rajani, B., 2000. Gray cast-iron water pipe metallurgy. J. Mater. Civ. Eng. 12 (3), 245–253. https://doi.org/10.1061/(asce)0899-1561(2000)12:3(245).

Mokhtari, M., Melchers, R.E., 2020. Reliability of the conventional approach for stress/fatigue analysis of pitting corroded pipelines – Development of a safer approach. Struct. Saf. 85, 101943. https://doi.org/10.1016/j.strusafe.2020.101943.

National Infrastructure Commission, 2018. Preparing for a drier future: england's water infrastructure needs [Report]. https://nic.org.uk/nic-preparing-for-a-drier-future-26-april-2018/.

Northumbrian Water, 2024. Price review 2024 (PR24) business plan tables (version 6) [data tables]. https://www.nwg.co.uk/globalassets/business-plan-2025-30/update-jan24/nes_bpt_01-pr24-bp-tables-v6—25-jan-2024-update-including-ntal-option-1.xlsb.

Pilkey, W.D., Pilkey, D.F., 2008. Peterson's Stress Concentration Factors, 3rd ed. John Wiley & Sons, Inc.

Pokorny, P., Vojtek, T., Náhlík, L., Hutar, P., 2017. Crack closure in near-threshold fatigue crack propagation in railway axle steel EA4T. Eng. Fract. Mech. 185, 2–19. https://doi.org/10.1016/j.engfracmech.2017.02.013.

Rajani, B., Tesfamariam, S., 2004. Uncoupled axial, flexural, and circumferential pipe-soil interaction analyses of partially supported jointed water mains. Can. Geotech. J. 41, 997–1010. https://doi.org/10.1139/T04-048.

Rathnayaka, S., Shannon, B., Jiang, R., Kodikara, J., 2018. New laboratory test facility developed to investigate the leak-before-break window of large-diameter cast iron water pipes. J. Pipeline Syst. Eng. Pract. 9 (3), 04018010. https://doi.org/10.1061/(asce)ps.1949-1204.0000329.

Rathnayaka, S., Shannon, B., Robert, D., Kodikara, J., 2017a. Experimental evaluation of bursting capacity of corroded grey cast iron water pipeline. Struct. Infrastruct. Eng. 13 (12), 1553–1562. https://doi.org/10.1080/15732479.2017.1303840.

Rathnayaka, S., Shannon, B., Zhang, C., Kodikara, J., 2017b. Introduction of the leak-before-break (LBB) concept for cast iron water pipes on the basis of laboratory experiments. Urban. Water. J. 14 (8), 820–828. https://doi.org/10.1080/1573062X.2016.1274768.

Rezaei, H., Ryan, B., Stoianov, I., 2015. Pipe failure analysis and impact of dynamic hydraulic conditions in water supply networks. Procedia Eng. 119 (1), 253–262. https://doi.org/10.1016/j.proeng.2015.08.883.

Robert, D.J., Chan, D., Rajeev, P., Rajalingam, J., Kodikara, J., 2020. Field evaluation of in-service buried pipeline using robust instrumentation. Transp. Geotech. 24, 100376. https://doi.org/10.1016/j.trgeo.2020.100376.

Sanders, J., Marshallsay, D., Mountfort, G., Fox, G., Butler, M., 2022. A leakage routemap to 2050 [Report]. https://www.water.org.uk/news-item/milestone-leakage-routemap-to-revolutionise-the-reduction-of-leakage-from-pipes/.

Seica, M.V., Packer, J.A., 2004. Mechanical properties and strength of aged cast iron water pipes. J. Mater. Civ. Eng. 16 (1), 69–77. https://doi.org/10.1061/(asce)0899-1561(2004)16:1(69).

Severn Trent Water, 2024. Price review 2024 (PR24) business plan tables (version 6) [data tables]. https://www.stwater.co.uk/content/dam/stw/about_us/pr24/sve40-data-tables.xlsb.

Smith, P., Topper, K., Watson, T., 1970. A stress–strain function for the fatigue of metals. J. Mater. 5 (4), 767–778.

Socie, D.F., Marquis, G.B., 1999. Multiaxial fatigue. SAE International. https://saemobilus-sae-org.sheffield.idm.oclc.org/content/R-234.

Soltani Asadi, Z., Melchers, R.E., 2018. Long-term external pitting and corrosion of buried cast iron water pipes. Corros. Eng. Sci. Technol. 53 (2), 93–101. https://doi.org/10.1080/1478422X.2017.1400291.

South West Water, 2024. Price review 2024 (PR24) business plan tables (version 6) [data tables]. https://www.southwestwater.co.uk/siteassets/documents/about-us/business-plans/2025-30/pr24-bptables-v6-publish—swb.xlsb.

Southern Water, 2024. Price review 2024 (PR24) business plan tables (version 7) [data tables]. https://www.southernwater.co.uk/about-us/our-plans/business-plan-2025-30/.

Stephens, M., Gong, J., Zhang, C., Marchi, A., Dix, L., Lambert, M.F., 2020. Leak-before-break main failure prevention for water distribution pipes using acoustic smart water technologies: case study in Adelaide. J. Water. Resour. Plan. Manage 146 (10), 05020020. https://doi.org/10.1061/(asce)wr.1943-5452.0001266.

Thames Water, 2024. Price review 2024 (PR24) business plan tables (version 8) [data tables]. https://www.thameswater.co.uk/media-library/home/about-us/regulation/our-five-year-plan/draftdetermination-2024/data-tables/TMS-DD-002-PR24-Draft-Determination-Data-Tablesfinal.xlsx.
UKWIR, 2021. National mains failure database (version 13/11/2024) [data set]. https://mainsfailuredatabase.ukwir.org/national-mains-failure-database-2021.
UN-Water, 2021. Summary progress update 2021: SDG 6 - water and sanitation for all [United Nations report]. https://www.unwater.org/sites/default/files/app/uploads/2021/12/SDG-6-Summary-Progress-Update-2021_Version-July-2021a.pdf.
United Utilities, 2024. Price review 2024 (PR24) business plan tables (version 28/08/2024) [data tables]. https://www.unitedutilities.com/globalassets/zcorporate-site/pr24/august-2024/data-and-models/uuwr_90_data-tables.xlsx.
Van Zyl, J.E., Malde, R., 2017. Evaluating the pressure-leakage behaviour of leaks in water pipes. J. Water Suppl. 66 (5), 287–299. https://doi.org/10.2166/aqua.2017.136.
Walat, K., Łagoda, T., 2014. Lifetime of semi-ductile materials through the critical plane approach. Int. J. Fatigue 67, 73–77. https://doi.org/10.1016/j.ijfatigue.2013.11.019.
Wallbrink, C., Hughes, J.M., Kotousov, A., 2023. Experimental investigation of crack opening loads in an aircraft load spectrum. Int. J. Fatig. 171, 107560. https://doi.org/10.1016/j.ijfatigue.2023.107560.
Weinacht, D.J., Socie, D.F., 1987. Fatigue damage accumulation in grey cast iron. Int. J. Fatig. 9 (2), 79–86. https://doi.org/10.1016/0142-1123(87)90048-X.
Wessex Water, 2024. Price review 2024 (PR24) business plan tables (version 6) [Data tables]. https://corporate.wessexwater.co.uk/media/toebmbhz/wsx46-data-tables.xlsb.
Xiao, C., Sun, R., Adrien, J., Lachambre, J., Nadot, Y., Weck, A., Buffière, J.Y., 2024. 3D characterization of closure of surface and internal fatigue cracks in nodular cast iron using Digital volume correlation of laboratory X-ray tomography images. Int. J. Fatig. 182, 108226. https://doi.org/10.1016/j.ijfatigue.2024.108226.
Yamamoto, K., Mizoguti, S., Yoshimitsu, K., Kawasaki, J., 1983. Relation between graphitic corrosion and strength degradation of cast iron pipe. Boshoku. Gijutsu. 32 (3), 157–162. https://doi.org/10.3323/jcorr1974.32.3_157.
Yorkshire Water, 2024. Price review 2024 (PR24) business plan tables (Version 7) [Data tables]. https://www.yorkshirewater.com/media/qkedhdk2/yky-pr24-ddr-63-data-tables-4.xlsb.
Yu, T., Chen, X., Yan, W., Xu, Z., Ye, M., 2023. Leak detection in water distribution systems by classifying vibration signals. Mech. Syst. Signal. Proc. 185, 109810. https://doi.org/10.1016/j.ymssp.2022.109810.
Zhang, C., Rathnayaka, S., Shannon, B., Ji, J., Kodikara, J., 2017. Numerical interpretation of pressurized corroded cast iron pipe tests. Int. J. Mech. Sci. 128 (129), 116–124. https://doi.org/10.1016/j.ijmecsci.2017.04.015.

Further reading

A video recording from which the stills in Fig. 5 were taken is provided to help readers visualise the process of leak evolution.